Journal of Materials Chemistry

Cite this: J. Mater. Chem., 2011, 21, 13991

www.rsc.org/materials

PAPER

Graphene/cellulose nanocomposite paper with high electrical and mechanical performances†

Nguyen Dang Luong,[a] Nikolaos Pahimanolis,[a] Ulla Hippi,[a] Juuso T. Korhonen,[b] Janne Ruokolainen,[b] Leena-Sisko Johansson,[c] Jae-Do Nam[d] and Jukka Seppälä*[a]

Received 13th May 2011, Accepted 17th June 2011
DOI: 10.1039/c1jm12134k

Graphene/cellulose nanocomposite paper with high mechanical and electrical performances was reported in this study by combining reduced graphene oxide sheets (RGO) and amine-modified nanofibrillated cellulose (A-NFC) in a well-controlled manner. By adjusting the GO content, various graphene/cellulose nanocomposites with 0.1–10 wt% content of graphene were obtained. The RGO/A-NFC nanocomposite synthesized by the developed method exhibits an electrical percolation threshold of 0.3 wt% with an electrical conductivity of 4.79×10^{-4} S m^{-1}, which is well above the antistatic value. Furthermore, with 10 wt% of graphene, a high conductivity of 71.8 S m^{-1} was measured for the nanocomposite. Moreover, it was found that on addition of only 0.3 wt% of graphene, the tensile strength increased by 1.2 fold and 2.3 folds compared to that of the neat cellulose and graphene oxide paper, respectively, revealing an excellent reinforcement of graphene sheets. Moreover, the elongation at break of the composite with graphene content was 8.5%, which is similar to that of A-NFC paper and much higher than that of GO paper. It is noteworthy to mention that with 5 wt% of graphene, the RGO/A-NFC composite paper showed a significantly enhanced tensile strength of 273 MPa that is 1.4 fold and 2.8 folds higher than that of the cellulose papers and graphene oxide paper, respectively. Such a high enhancement of electrical and mechanical properties in cellulose paper by graphene has never been reported before for any carbon-based material/cellulose composite paper.

Introduction

Graphene is the building block for other graphitic carbons of zero-dimension fullerene, one-dimension carbon nanotubes, and three-dimension graphite and its existence was recently proved in 2004.[1] Graphene exhibits exceptional physical properties, *e.g.*, electron mobility of 200 000 cm^2 V^{-1} s^{-1},[2] room-temperature fractional quantum Hall effects,[3] and the highest mechanical property values ever measured with 1 TPa Young's modulus and 130 GPa ultimate strength.[4] It also has an outstanding thermal conductivity of around 5000 Wm^{-1} K^{-1}, which is higher than that of carbon nanotubes or diamond.[5] Thus, graphene has been intensively used to develop a wide range of novel functional materials for various applications, such as ultracapacitors,[6] transparent conducting electrodes,[7,8] antibacterial materials,[9] and polymer composites.[10]

Graphene can be prepared by both bottom-up (such as chemical vapor deposition, arc-discharge, unzipping carbon nanotube, and epitaxial growth on SiC) and top-down (thermal and chemical reduction of exfoliated graphite derivatives, such as graphene oxide) approaches.[11] Among them, the top-down approach, starting from graphene oxide, is the most promising method for potential uses in polymer composites. There are two important reasons: (1) graphene oxide is readily dispersible in water and easily modified to be dispersed in both polar and non-polar polymer matrices, and (2) graphite with a global production of more than 1.1 million tons and 825 $ per ton in 2008.[11]

Recently, researchers have shown an increased interest in graphene-based composite development in which graphene sheets are used to enhance mechanical properties and electrical conductivity simultaneously.[11] For example, an electrically conductive graphene/polystyrene composite was prepared by solution mixing in DMF of exfoliated phenyl isocyanate-treated graphite oxide sheets with polystyrene, followed by their

[a]*Polymer Technology, Department of Biotechnology and Chemical Technology, Aalto University, School of Chemical Technology, P.O. Box 16100, 00076 Aalto, Finland. E-mail: jukka.seppala@aalto.fi; Fax: +358 9 451 2622; Tel: +358 9 470 22614*
[b]*Molecular Materials, Department of Applied Physics, Aalto University, School of Science, P.O.Box 15100, 00076 Aalto, Finland*
[c]*Forest Products Surface Chemistry Group, Department of Forest Products Technology, Aalto University, School of Chemical Technology, P.O.Box 16300, 00076 Aalto, Finland*
[d]*Department of Polymer Science and Engineering, Sungkyunkwan University, Suwon, 440-746, South Korea*
† Electronic supplementary information (ESI) available: Experiment and characterization of A-NFC material. See DOI: 10.1039/c1jm12134k

chemical reduction by dimethylhydrazine.[10] The graphene/polystyrene composite exhibits a percolation threshold of 0.1 volume percent for electrical conductivity, the lowest value for carbon-based composites. In another example of major difference in properties with a small graphene addition, the authors reported that only 1 wt% and 0.05 wt% of functionalized graphene sheets in poly(acrylonitrile) and poly(methyl methacrylate) increase the glass transition temperature of the composite over 40 °C and 30 °C, respectively.[12]

Cellulose is renewable, biodegradable and it is the most abundant natural polymer, with a quantity of 10^{11} tons per year.[13] In wood pulp, cellulose is organized as aggregates of nanofibrils in the lignin matrix. Cellulose nanofibrils were first isolated from wood pulp in 1983.[14] However, the isolation process was only recently achieved in high quality in 2007.[15] Nanofibrillated cellulose (NFC) offers transparency, biocompatibility, and excellent mechanical properties, for example, a theoretical Young's modulus of 167.5 GPa for the native perfect crystal, which is higher than that of steel and similar to that of Kevlar.[16] These outstanding properties make nanofibrillated cellulose a good candidate in various advanced materials for biomaterials and electronic devices.

Carbon nanotubes (CNTs) have been incorporated with cellulose paper in many applications, such as electromagnetic interference shielding,[17,18] and energy storage devices.[19] However, so far, there has been no report on graphene/cellulose composite paper. Therefore, in this study, we report the properties of graphene/cellulose nanocomposite papers made by filtering stable reduced graphene oxide/cellulose emulsions. Both tensile strength and modulus of the graphene/composite papers are dramatically increased in comparison with that of graphene oxide and neat cellulose papers. Furthermore, the graphene composite paper exhibits a low percolation threshold of electrical conductivity at 0.3 wt% of graphene loading. With graphene loading in a range of 0.1–10 wt%, the electrical conductivity of the graphene/cellulose composite was easily controlled between 4.79×10^{-4} S m^{-1} and 71.8 S m^{-1}, which is sufficient for many electrical applications. Due to the good physical and electrical properties, the graphene/cellulose composite paper developed herein may potentially be used in portable and bendable electronic equipment such as rollup displays and wearable devices.[8,20] Particularly, stable graphene/cellulose dispersions, similar to carbon nanotube dispersions, could be easily achieved and scalable; hence, they may be used as conductive inks for various purposes.[19,21]

Experimental section

Materials

Graphite flake (particle size <150 μm), sulfuric acid (98%), chlorhydric acid (36 wt%), hydrogen peroxide (36 wt%), potassium permanganate, sodium nitrate, A-NFC suspension, ammonia solution (25 wt%), and hydrazine solution (60 wt%) were purchased from Sigma-Aldrich Co. Amine-functionalized nanofibrillated cellulose (A-NFC) was prepared from a nanofibrillated cellulose (NFC) suspension.[22] Detailed experiment and characterization of A-NFC material are presented in the ESI†.

Preparation of graphene oxide dispersion

Graphite oxide was prepared by a modified Hummers method.[23] Briefly, 10 g of graphite flake, 5 g of sodium nitrate, and 30 g of potassium permanganate were added to 250 ml of sulfuric acid slowly and the mixture was stirred in an ice bath. The mixture was then heated to 35 °C for 2 h to further oxidize the graphite. Then, 500 ml of deionized water was slowly added into the mixture and kept for 30 min. 30 ml of H_2O_2 (36 wt%) was added into the reaction. After that the mixture was diluted in 2000 ml of HCl (10 wt%) and filtered. Subsequently, the mixture was washed several times with DI water until pH 7. Finally, the graphite oxide product was dried at 100 °C for 48 h. To obtain graphene oxide dispersion, graphite oxide powder was added into DI water (1 mg ml^{-1}) and sonicated for 1.5 h. The graphene oxide solution was then obtained by centrifuging the sonicated mixture at 4000 rpm for 20 min to remove the precipitates.

Preparation of reduced graphene oxide/A-NFC composites

A variety of graphene oxide dispersions (0.4 mg ml^{-1}) were controllably added to A-NFC (1.32 wt%, 20 g) suspensions to have mixtures with graphene content from 0.1–10 wt% under stirring. To each reaction mixture, 0.1 ml of ammonia solution (25 wt%) was added and the mixtures were then vigorously stirred at 70 °C for 1 h. Then, 0.2 ml of hydrazine was added and the reactions were heated to 95 °C and kept stirred for 2 h to reduce the graphene oxide. RGO/A-NFC composite papers were prepared by filtration of the obtained solution through a mixed cellulose ester membrane (47 mm in diameter, 0.45 μm pore size, Whatman, Germany) and washing three times with DI water to eliminate impurities. The papers were finally peeled off from the filter paper and dried for 48 h. NFC and A-NFC papers were also prepared by filtration.

Characterization

X-Ray diffraction of the samples were carried out on a wide angle X-ray diffractor (Mac Science, Mac-18xhf) with Cu Kα radiation ($\lambda = 0.154$ nm) and data were collected in the 2θ of 5–50° with a scanning speed of 5° min^{-1}.

Raman spectra were collected from 1000 to 2000 cm^{-1} using a micro-Raman spectrometer (Jobin Yvon LabRam 300) with an excitation wavelength of 633 nm. Fourier transform infrared spectroscopy (FT-IR) was conducted on a FTIR-ATR-MATTSON 3000-FTIR spectrometer. The morphology of the samples was studied by a field emission scanning electron microscope (FE-SEM, JEOL JSM-7500FA) at 5 kV, and a transmission electron microscope (JEOL JEM 2100–2100F) at 200 kV. Tensile test of the film samples of 20 × 0.02 × 5.3 cm^3 (length × thickness × width) was characterized using an Instron 4204 universal testing machine with a test speed of 0.05 mm min^{-1} for the graphene oxide paper and 0.5 mm min^{-1} for other samples. At least five specimens were used for each sample in the tensile test. The thickness of the samples was controlled to be around 20 μm. To study the fracturing of the composites, the specimens were fractured using a tensile tester and the exposed cross-sections were sputtered with a thin layer of platinum (Emitech K100X) to promote conductivity before SEM observation. Electrical conductivity of the samples was measured by a four-point probe

method from Jandel Engineering Ltd. connected to a Keithley 2400 source meter using a standard four-probe technique with a threshold detection limit of 100 MΩ. Chemical composition of the sample surfaces was studied by high resolution X-ray photoelectron spectroscopy (XPS, AXIS 165, Kratos Analytical), using monochromated Al Kα irradiation at 100 W, and an *in situ* reference of pure cellulose.[24] The C–O bond of the cellulose at 286.6 eV was used as the reference value for binding energy corrections.[25]

Results and discussion

Fig.1 shows XRD patterns (A) and Raman spectra (B) for pristine graphite (a) and graphene oxide (b). In Fig. 1A (a), the pristine graphite has a sharp and strong peak at 26.4°, indicating the characteristic peak of the graphene layers in graphite. However, the XRD pattern of the GO sheets (b) shows only a very minor peak at 11.0°. The disappearance of the 26.4° peak is due to the formation of various functional groups, such as epoxide and carboxyl functionalities during the chemical oxidation and then forcing the ordered layers to diverge.[26] As seen in Fig. 1B, the Raman spectrum of graphite (a) exhibits a strong G band at 1571 cm^{-1} regarded as the characteristic peak of graphite structure, and a minor D band at 1326 cm^{-1}. In the Raman spectrum of the graphene oxide (b), appearance of a prominent D band at 1336 cm^{-1} is due to the disordered structure of the graphene oxide sheets, probably caused by the oxygen functionalities on the surface during the oxidation. Moreover, the G band of the graphene oxide is shifted to 1594 cm^{-1}, possibly due to the electron-accepting oxygen functionalities.[27,28] Additionally, the morphology of the GO sheets was shown in the SEM (C) and TEM (D) images, which exhibit a folded feature and verify the formation of individual GO sheets. The high aspect ratio of graphene oxide sheets thus should be beneficial in composite

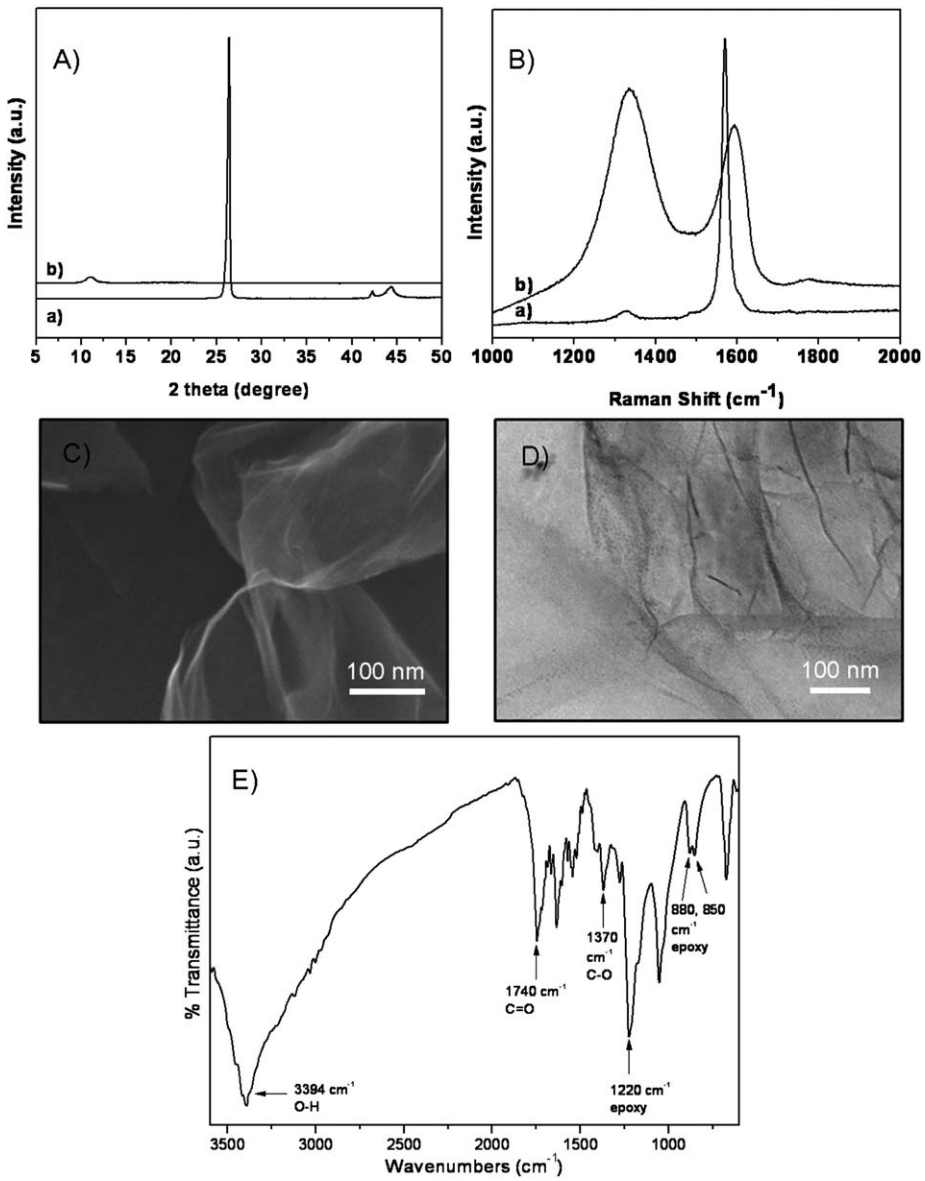

Fig. 1 XRD (A) and Raman (B) spectra of graphite (a) and graphene oxide samples (b). High magnification SEM image of GO with Pt coating before the observation (C) and TEM (D) images showing the morphology of graphene oxide sheets. (E) FT-IR spectrum of graphene oxide powder.

materials to enhance mechanical strength and generate electrical conductivity. Furthermore, FT-IR spectra of GO (Fig. 1E) present three peaks at 1220 cm^{-1}, 880 cm^{-1} and 850 cm^{-1} of epoxy groups, which are corresponding to symmetric stretching, asymmetric stretching, and deformation modes, respectively. The 1740 cm^{-1}, 1370 cm^{-1}, and 3394 cm^{-1} bands are attributed to C═O (carboxy/carbonyl), C–O vibration, and O–H stretching vibration, respectively.[26] Taking all five analyses above together, we can confirm that individual GO sheets were successfully prepared by the chemical oxidation and ultrasonication treatments in this study.

Graphene oxide sheets contain a number of functional epoxy groups on the basal plane,[29] which can be opened by amine species as nucleophiles;[26,30] therefore, it is assumed that the epoxy functionalities on the GO sheets would react with amine in the A-NFC to form covalent bonding through the amine-epoxide reaction, creating new C–N bonds between graphene sheets and A-NFC fibrils. Thus, XPS was used in this study to evaluate the interaction between graphene oxide sheets and A-NFC in the RGO/A-NFC composites. Fig. 2 shows energy-corrected high resolution XPS spectra of the N 1s (A), C 1s (B), and O 1s (C) regions for GO paper (a), A-NFC paper (b), GO/A-NFC composite paper (c), and RGO/A-NFC composite paper (d). In Fig. 2A, all three curves for A-NFC, GO/A-NFC, and RGO/A-NFC samples show the peaks for the N 1s and this is not the case for the GO paper (a), confirming the presence of nitrogen atoms in the A-NFC, GO/A-NFC, and RGO/A-NFC. In Fig. 2B, there are marked differences in the carbon region: a strong C–O peak in the GO paper indicates significant oxidation, the C–O and O–C–O compounds in a ratio typical of cellulose are the main feature in the A-NFC, the GO/A-NFC composite paper shows both features while the carbon in the RGO/A-NFC composite is clearly reduced and has a clear peak shape. As expected, the CC signal in samples with graphitic carbon is shifted to lower binding energy, when compared to the organic passivation layer seen in the cellulose sample.[25] In addition, the intensity of the C–O peak was decreased in the GO/A-NFC and RGO/A-NFC. This observation may be evidence for the reaction between carboxylic acid and amine groups.[30,31] However, further study should be conducted in this matter. The last XPS surveys (Fig. 2C) show that the peak intensity of O 1s in the RGO/A-NFC composite is much smaller than that of the un-reduced GO/A-NFC material; together with the carbon data it confirms that the reduction of graphene oxide was effective in restoring the conjugated graphitic structure through the chemical reduction with hydrazine.

Reduction of graphene oxide in the GO/A-NFC mixtures by hydrazine was carried out in the presence of ammonia to maintain the pH in a range of 10–12; thereby the forming individual graphene sheets can be stabilized effectively in the solution through an electrostatic stabilization.[32] The color change from light brown to black clearly indicated the formation of graphene as seen in the photograph of an RGO/A-NFC with 10 wt% of graphene content in a 100 ml flask (Fig. 3A, right). Although further research should be conducted, the RGO/A-NFC dispersions described herein may be used as conductive inks.[19] Photographs of RGO/A-NFC nanocomposite papers with various graphene loadings are shown in Fig. 3A (right). With only 0.3 wt% graphene loading, the color of the composite paper was dark, compared with the white color of the neat A-NFC paper. Further increase in the graphene contents to 1 wt%, 5 wt %, and 10 wt%, the color of nanocomposite papers became darkened further. Combined with the XPS result, we can conclude that the GO sheets simultaneously experienced a partial reduction process upon the chemical reduction with ammonia and hydrazine solutions.

To evaluate the reinforcement of graphene in the graphene/A-NFC composites, tensile testing of these papers was

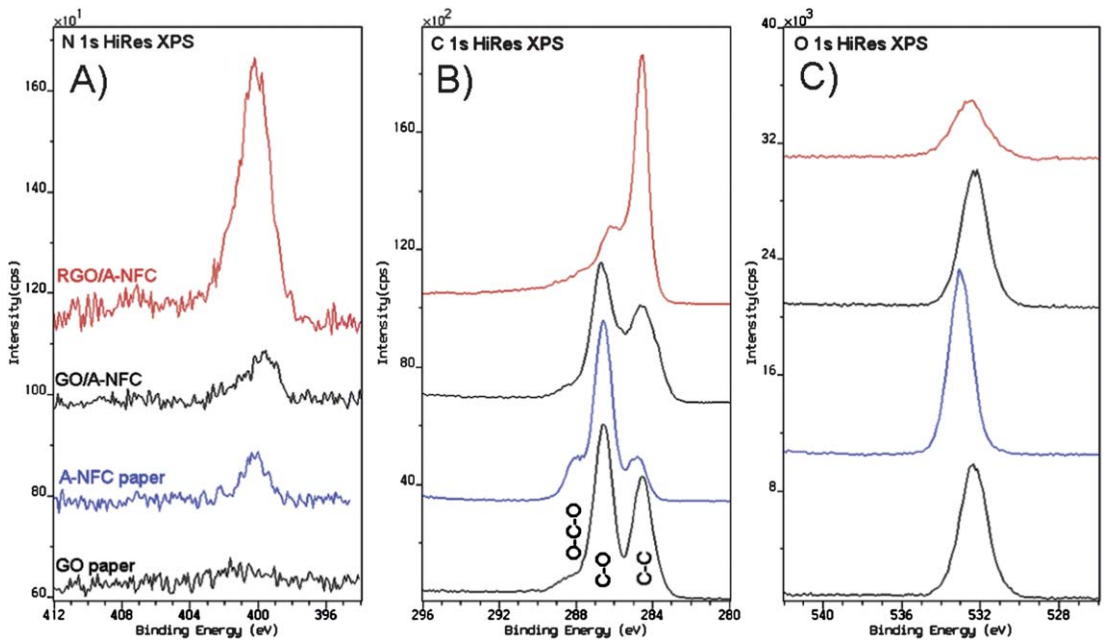

Fig. 2 N 1s (A), C 1s (B), and O 1s (C) XPS results for GO paper, A-NFC paper, GO/A-NFC composite paper, and RGO/A-NFC composite paper using a 50/50 weight ratio of GO/A-NFC for the easy observation.

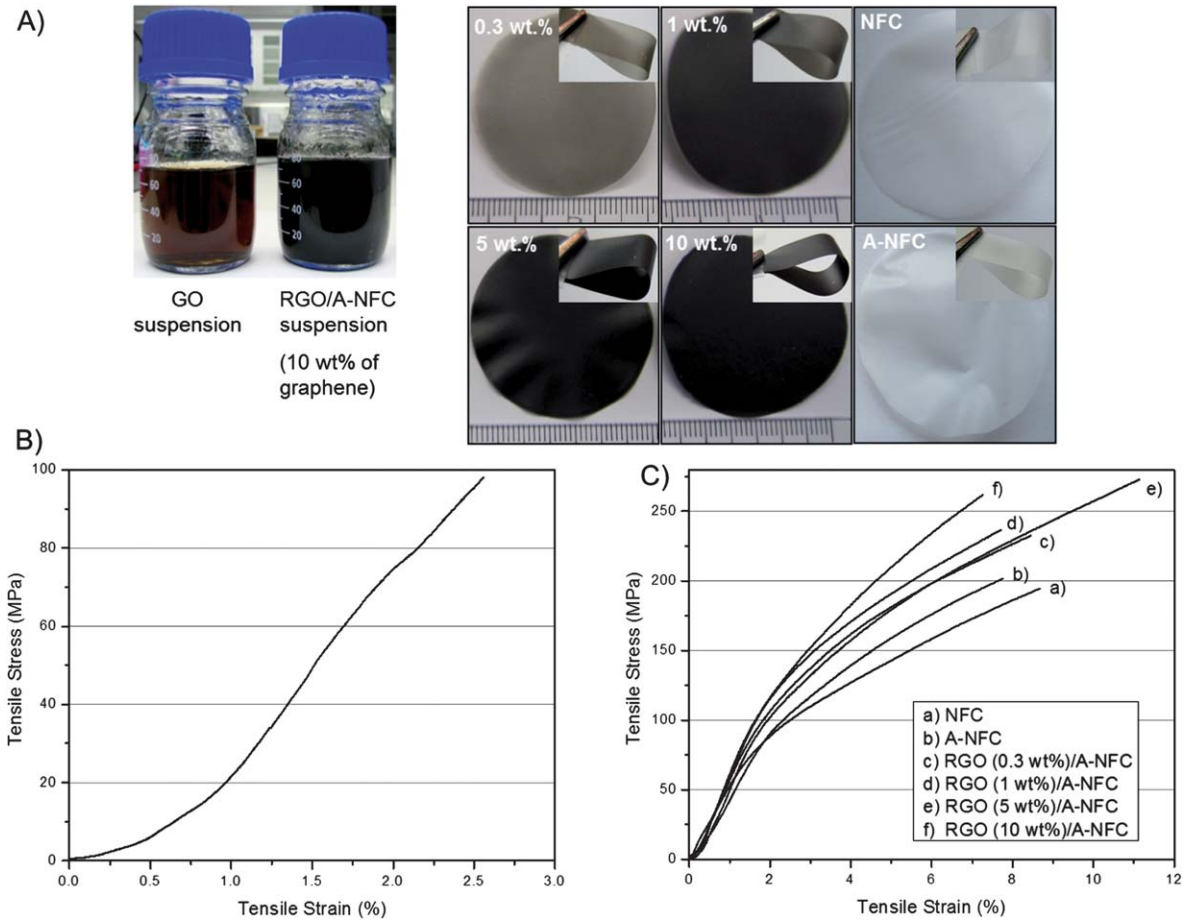

Fig. 3 (A) Photos of GO solution (0.4 mg ml^{-1}) and RGO/A-NFC (10 wt%) solution (right) in two 100 ml beakers and (left): NFC, A-NFC and RGO/A-NFC papers with some different graphene contents of 0.3 wt%, 1 wt%, 5 wt%, and 10 wt% showing the different levels of black color caused by the RGO contents, and the insets in the pictures exhibiting high flexibility of the composite papers. Typical stress–strain curves of graphene oxide paper (B) and (C) containing NFC (a) A-NFC (b) and RGO/A-NFC nanocomposite papers with graphene contents of 0.3 wt%, 1 wt%, 5 wt%, and 10 wt% (c–f, respectively).

conducted and the representative stress–strain curves are shown in Fig. 3B and C: graphene oxide in Fig. 3B, NFC (a) A-NFC (b) and RGO/A-NFC composites with 0.3 wt%, 1 wt%, 5 wt%, and 10 wt% of graphene loadings (c–f, respectively) in Fig. 3C. As mentioned before in the characterization section, two different testing speeds of 0.05 mm min^{-1} and 0.5 mm min^{-1} were applied to GO paper and the others, respectively, because the GO paper has very low strain at break. As seen in Fig. 3C, the graphene oxide paper exhibits a tensile strength of 98 MPa, an elastic modulus of 5.8 GPa, and a low strain at break of around 2.5%, which are comparable to that of graphene oxide paper prepared by Ruoff and co-workers.[30] In Fig. 3D, NFC and A-NFC samples show tensile strengths of 194 MPa, and 202 MPa, and moduli of 5.8 GPa and 5.4 GPa, respectively. Apparently, both NFC and A-NFC papers are roughly two times higher in tensile strength than that of graphene oxide paper. However, adding only 0.3 wt% of graphene in A-NFC suspension, the obtained RGO/A-NFC composite paper shows enhanced tensile strength and modulus of 232 MPa and 6.4 GPa, respectively, which correspond to 1.2 fold and 2.3 folds higher than that of the cellulose paper and graphene oxide paper, respectively. Further increasing graphene loading to 1 wt %, the tensile strength is almost unchanged, but the modulus is significantly increased to 7.1 GPa. Remarkably, when the graphene content increases to 5 wt%, the tensile strength impressively increases to 273 MPa, which is 2.8 folds and 1.4 fold higher than that of the graphene oxide paper and NFC/A-NFC papers, respectively. Undoubtedly, the excellent reinforcement in both tensile strength and modulus of the RGO/A-NFC papers could be attributed to the good dispersion of both RGO sheets and A-NFC fibrils in the composites, together with strong chemical/physical interactions between them. However, increasing the graphene content to 10 wt%, the tensile properties are not improved any more. The limitation of the enhancement in tensile properties at this content of graphene may be caused by the agglomeration of graphene sheets in the composite at 10 wt% of graphene loading.

SEM images shown in Fig. 4 were taken at the fractured surfaces of the tensile testing specimens to study the interfacial interaction between the graphene sheets and A-NFC fibrils, between cellulose fibrils in NFC and A-NFC paper, as well as between the GO sheets in GO paper. In Fig. 4A, the flat and smooth fractured surface of the GO paper is due to the low elongation at break of 2.5% and is consistent with the tensile

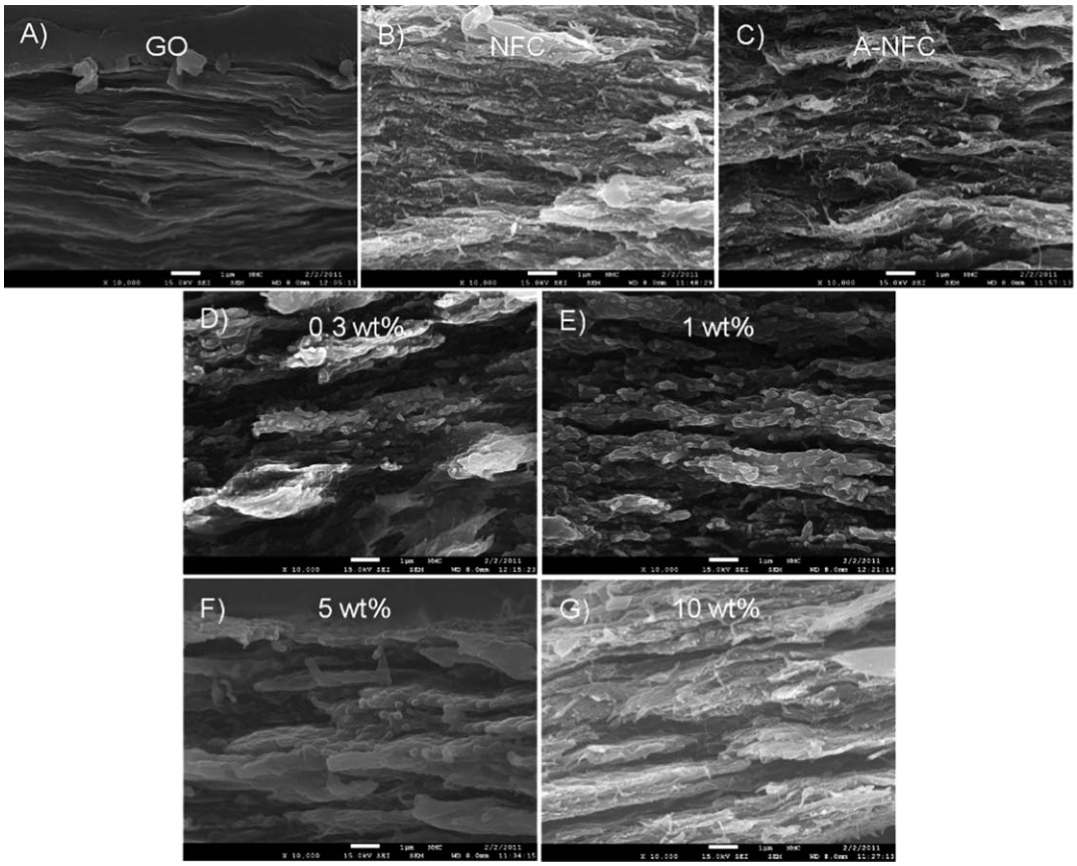

Fig. 4 SEM images of graphene oxide paper, NFC paper, A-NFC paper, and RGO/A-NFC nanocomposite paper with 0.3 wt%, 1 wt%, 5 wt%, and 10 wt% of graphene loadings (A–G, respectively), all taken at fractured sample surfaces upon tensile testing. All scale bars are 1 μm.

test, indicating the brittleness of the GO material. Moreover, the layered structure of the GO paper was possibly caused by the directional flow induced by vacuum filtration, which was also observed for the RGO/A-NFC composite papers. However, the fracture surfaces of the NFC, A-NFC, and RGO/A-NFC samples are rough, revealing a strong adhesion between NFC/A-NFC fibrils as well as graphene sheets and A-NFC fibrils, thus, being favorable to stress transfer to both components. It should be noted that both graphene sheets and cellulose fibrils have individually good mechanical properties and good adhesion between them would show an improvement in the properties of the forming composite materials. For example, in the RGO/A-NFC composites, graphene sheets and A-NFC nanofibrils are evenly dispersed through each other and bonded strongly through hydrogen bonding and chemical bonding as confirmed by XPS leading to the improvement in mechanical properties of the composites over GO, NFC and A-NFC papers.

As measured, GO, NFC, and A-NFC samples were not electrically conductive. The incorporation of graphene sheets into the A-NFC matrix also generates electrical conductivity of the cellulose composite papers. Electrical conductivity of the RGO/A-NFC samples as a function of graphene weight fraction is shown in Fig. 5. With the sample containing 0.1 wt% of graphene, electrical conductivity was not detected. However, as can be seen clearly, a sharp increase in electrical conductivity was observed between 0.1 and 0.3 wt% of graphene loadings. This increase in conductivity suggests that an infinite network of percolated graphene started to form between 0.1 and 0.3 wt%. The conductivity of the composite, σ, above the percolation threshold obeys a power law, $\sigma = \sigma_0 [(\theta - \theta_c)/(1 - \theta_c)]^t$, where σ_0 is the conductivity of the filler, θ is the filler fraction, θ_c is the percolation threshold, and t is the critical exponent.[33] The inset in Fig. 5 demonstrates the double-logarithmic plot of σ *versus* $(\theta - \theta_c)$ with the case $\theta_c = 0.3$ wt%, which was predicted by the power law equation and fitted to the experimentally measured conductivity. A low value of 0.3 wt% of graphene is found herein as the percolation value of conductivity for the RGO/A-NFC nanocomposites. As seen, at a graphene loading of 0.3 wt%, the conductivity of the composite was measured to be 4.79×10^{-4} S m^{-1}, which is well above the antistatic criterion of 10^{-6} S m^{-1}.[10] At a graphene content of only 3 wt%, the conductivities were measured to be 1.1 S m^{-1}. A remarkably high electrical conductivity value of 71.8 S m^{-1} of the composite paper with 10 wt% of graphene could be attributed to an effective recovery of the sp^2 network of carbon *via* the chemical reduction and a good graphene particle-to-particle connection in the composite paper. It should be addressed that the conductivities of our graphene-based composites, with graphene loading in the range of 0.3–3 wt%, are similar to those reported with polystyrene/graphene composites.[10] Notably, the polystyrene/graphene composite conductivities are comparable with the best values

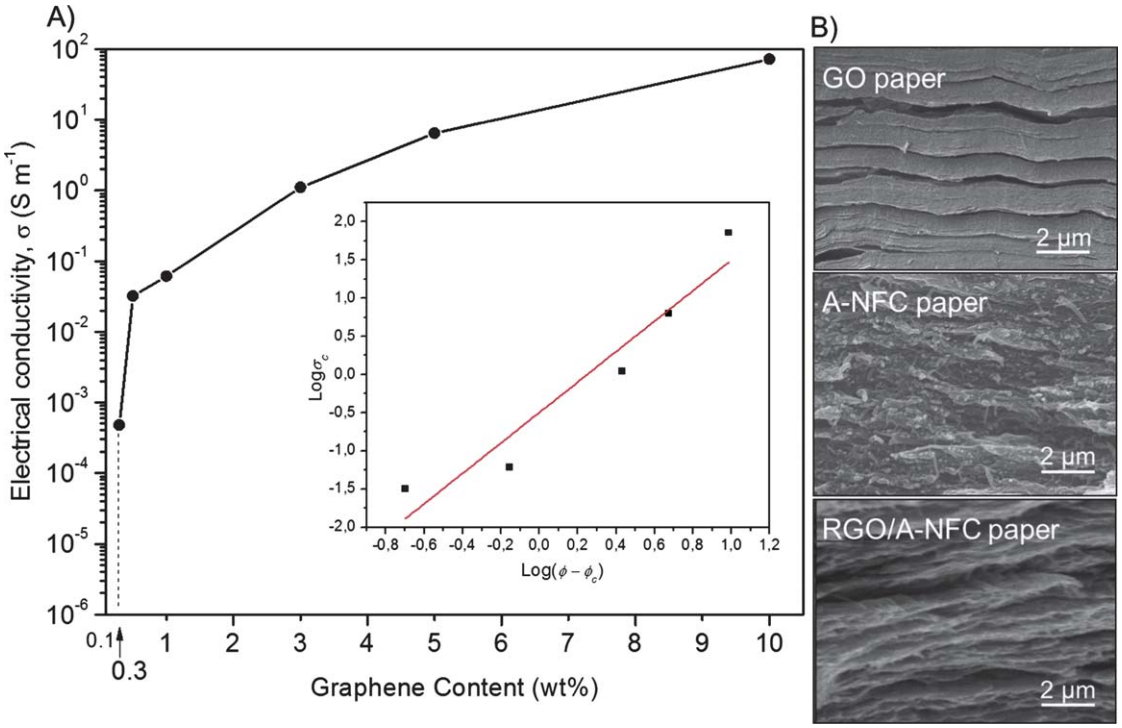

Fig. 5 (A) Semi-log plot of electrical conductivity of the RGO/A-NFC nanocomposite papers as a function of graphene weight fraction. The inset is a double-logarithmic plot of volume electrical conductivity σ *versus* $(\theta - \theta_c)$ with fitted parameters: $t = 1.99 \pm 0.32$, $\theta_c = 0.3$ wt%. (B) SEM images of GO paper, A-NFC paper, and RGO/A-NFC composite paper with 0.3 wt% of graphene loading showing a continuous network of graphene incorporated with A-NFC nanofibrils in the composite paper, observed at fractured surfaces.

reported for carbon nanotube/polymer composites. SEM images in Fig. 4B compare the morphology of RGO/A-NFC composite paper containing 0.3 wt% of graphene with GO paper and A-NFC paper at cross-sectioned surfaces, which were obtained by fracturing the neat films. SEM image of the RGO/A-NFC composite confirms that individual graphenes are uniformly dispersed to form a continuous network in the composite, giving the high electrical conductivity of the papers as confirmed by the measurements. In general, the low percolation threshold and high conductivity of the composite papers are obviously attributed to the excellent homogeneous dispersion of the extremely high aspect ratio graphene sheets in these composites, forming an effectively conductive 3D network, even at a low graphene loading of 0.3 wt%.

Graphene sheets have advantages over carbon nanotubes as indicated by previous studies.[12,34] These advantages are high specific surface area (calculated value of 2630 $m^2 g^{-1}$),[6] rough and wrinkled surface and unique flexible two-dimensional geometry. A nano-sized wrinkled and rough surface, caused by a high density of surface defects, may enhance mechanical interlocking with polymer molecules, leading to strong adhesion at the interface. Similarly, high surface area of the graphene sheets could result in high geometric constraint to the polymer chains. Therefore, it is worthwhile to mention that the efficiency of graphene in enhancing mechanical properties and conductivity of the cellulose composites is equal or even much better than that of CNTs.[10,12] For example, compared with that of a CNT/cellulose composite paper,[18] the conductivity values of our papers are similar. Moreover, the tensile strength of the CNT/cellulose papers is not improved by the incorporated CNTs. Adding more than 5 wt% of CNT, the tensile strength of the paper even decreased, which is not the case with graphene as shown in this study. In another study, SWCNT/cellulose papers that were incorporated with 35 wt% single wall CNTs give conductivities in a range of 3.52×10^{-3}–1.34 S m^{-1}, which are at least 5 fold lower than that of our RGO/A-NFC paper containing only 5 wt% of graphene.[35] These examples clearly indicate that the incorporation of graphene sheets into the cellulose matrix far outperform CNTs in terms of electrical properties and/or mechanical properties.

Conclusions

We report herein a facile approach to fabricate mechanically robust and electrically conductive materials based on amine functionalized cellulose nanofibrils and chemically reduced graphene oxide sheets. The RGO/A-NFC composites not only exhibit good electrical properties but also excellent mechanical properties. The significant enhancement in the mechanical properties and electrical conductivity of the RGO/A-NFC composites could be attributed to the good dispersion of high aspect ratio graphene sheets and A-NFC fibrils resulting in the formation of strong physical hydrogen bonding, interlocking, together with the chemical bonding between them. We believe that the composite paper described herein could find various applications in portable and bendable electronics, electromagnetic interference (EMI) shielding devices and electromagnetic pulse (EMP) protection.

Acknowledgements

The Finnish Center for Nanocellulose Technologies is acknowledged for delivering nanofibrillated cellulose. The work has been partly carried out as part of the project "Tailoring of nanocellulose structures for industrial applications (NASEVA) funded by the Finnish Funding Agency for Technology and Innovation (TEKES). Dr Joseph M. Campbell at the Aalto University is acknowledged for performing the high resolution XPS measurements. Dr Maoshuai is acknowledged for the help in Raman analysis and Mr Matti Lehtimäki is appreciated with XRD characterization.

References

1 A. K. Geim and K. S. Novoselov, *Nat. Mater.*, 2007, **6**, 183–191.
2 K. I. Bolotin, K. J. Sikes, Z. Jiang, M. Klima, G. Gudenberg, J. Hone, P. Kim and H. L. Stormer, *Solid State Commun.*, 2008, **146**, 351–355.
3 Y. Zhang, Y. W. Tan, H. L. Stormer and P. Kim, *Nature*, 2005, **438**, 201–204.
4 C. Lee, X. Wei, J. W. Kysar and J. Hone, *Science*, 2008, **321**, 385–388.
5 A. A. Baladin, S. Gosh, W. Bao, I. Calizo, D. Teweldebrhan, F. Miao and C. N. Lau, *Nano Lett.*, 2008, **8**, 902–907.
6 M. D. Stoller, S. Park, Y. Zhu, J. An and R. S. Ruoff, *Nano Lett.*, 2008, **8**, 3498–3502.
7 X. Wang, L. Zhi and K. Mullen, *Nano Lett.*, 2008, **8**, 323–327.
8 G. Eda, G. Fanchini and M. Chhowalla, *Nat. Nanotechnol.*, 2008, **3**, 270–274.
9 W. Hu, C. Peng, W. Luo, M. Lv, X. Li, D. Li, Q. Huang and C. Fan, *ACS Nano*, 2010, **4**, 4317–4323.
10 S. Stankovich, D. A. Dikin, G. H. B. Dommett, K. M. Kohlhaas, E. J. Zimney, E. A. Stach, R. D. Piner, S. B. T. Nguyen and R. S. Ruoff, *Nature*, 2006, **442**, 282–286.
11 H. Kim, A. A. Abdala and C. W. Macosko, *Macromolecules*, 2010, **43**, 6515–6530.
12 T. Ramanathan, A. A. Abdala, S. Stankovich, D. A. Dikin, M. Herrera-Alonso, R. D. Piner, D. H. Adamson, H. C. Schniepp, X. Chen, R. S. Ruoff, S. T. Nguyen, I. A. Aksay, R. K. PrudHomme and L. C. Brinson, *Nat. Nanotechnol.*, 2008, **3**, 327–331.
13 T. Zimmermann, N. Bordeanua and E. Strub, *Carbohydr. Polym.*, 2010, **79**, 1086–1093.
14 A. F. Turbak, F. W. Snyder and K. R. Sandberg, *J. Appl. Polym. Sci.: Appl. Polym. Symp.*, 1983, **37**, 815–827.
15 S. Iwamoto, A. N. Nakagaito and H. Yano, *Appl. Phys. A: Mater. Sci. Process.*, 2007, **89**, 461–466.
16 K. Tashiro and M. Kobayashi, *Polymer*, 1991, **32**, 1516–1526.
17 B. Fugetsu, E. Sano, M. Sunada, Y. Sambongi, T. Shibuya, X. Wang and T. Hiraki, *Carbon*, 2008, **46**, 1256–1258.
18 M. Imai, K. Akiyama, T. Tanaka and E. Sano, *Compos. Sci. Technol.*, 2010, **70**, 1564–1570.
19 L. Hu, M. Pasta, F. La Mantia, L. F. Cui, S. Jeong, H. D. Deshazer, J. W. Choi, S. M. Han and Y. Cui, *Nano Lett.*, 2010, **10**, 708–714.
20 H. Gwon, H. S. Kim, K. U. Lee, D. H. Seo, Y. C. Park, Y. S. Lee, B. T. Ahn and K. Kang, *Energy Environ. Sci.*, 2011, **4**, 1277–1283.
21 L. Hu, J. W. Choi, Y. Yang, S. Jeong, F. L. Mantia, L. F. Cui and Y. Cui, *Proc. Natl. Acad. Sci. U. S. A.*, 2009, **106**, 21490–21494.
22 N. Pahimanolis, A. H. Vesterinen, J. Rich and J. Seppala, *Carbohydr. Polym.*, 2010, **82**, 78–82.
23 W. S. Hummers and R. E. Offemam, *J. Am. Chem. Soc.*, 1958, **80**, 1339.
24 L. S. Johansson and J. M. Campbell, *Surf. Interface Anal.*, 2004, **36**, 1018–1022.
25 G. Beamson and D. Briggs, *Cellulose Spectra in High Resolution XPS of Organic Polymers: The Scienta ESCA300 database*, Chisester, 1992.
26 J. Oh, J. H. Lee, J. C. Koo, H. R. Choi, Y. K. Lee, T. Kim, N. D. Luong and J. D. Nam, *J. Mater. Chem.*, 2010, **20**, 9200–9204.
27 K. N. Kudin, B. Ozbas, H. C. Schniepp, R. K. Prud'homme, I. A. Aksay and R. Car, *Nano Lett.*, 2008, **8**, 36–41.
28 S. Stankovich, D. A. Dikin, R. D. Piner, K. A. Kohlhaas, A. Kleinhammes, Y. Jia, Y. Wu, S. B. T. Nguyen and R. S. Ruoff, *Carbon*, 2007, **45**, 1558–1565.
29 H. He, J. Klinowski, M. Forster and A. Lerf, *Chem. Phys. Lett.*, 1998, **287**, 53–56.
30 S. Park, D. A. Dikin, S. B. T. Nguyen and R. S. Ruoff, *J. Phys. Chem. C*, 2009, **113**, 15801–15804.
31 K. Nakamoto, *Infrared and Raman Spectra of Inorganic and Coordination Compounds*, John Wiley & Sons, New York, 4th edn, 1986.
32 D. Li, M. B. Muller, S. Gilje, R. B. Kaner and G. G. Wallace, *Nat. Nanotechnol.*, 2008, **3**, 101–105.
33 D. S. Mclachlan, C. Chiteme, C. Park, K. E. Wise, S. E. Lowther, P. T. Lillehei, E. J. Siochi and J. S. Harrison, *J. Polym. Sci., Part B: Polym. Phys.*, 2005, **43**, 3273–3287.
34 M. A. Rafiee, J. Rafiee, Z. Wang, H. Song, Z. Z. Yu and N. Koratkar, *ACS Nano*, 2009, **3**, 3884–3890.
35 R. E. Anderson, J. Guan, M. Ricard, G. Dubey, J. Su, G. Lopinski, G. Dorris, O. Bourne and B. Simard, *J. Mater. Chem.*, 2010, **20**, 2400–2407.

